Article

Impact of Pyrite Oxidation on the Pore-Structure Characteristics of Shale Reservoir Rocks under the Interaction of Fracturing Fluid

Zepeng Sun, Yue Ni,* Yuandong Wu, and Yong Lei

Read Online

ACCESS | Metrics & More | Article Recommendations

ABSTRACT: Hydraulic fracturing combined with horizontal drilling is widely used to develop shale gas resources, and huge amounts of fracturing fluid are injected into shale reservoirs. However, the fracturing fluid is ineluctably retained in reservoir rocks after fracturing, resulting in the alteration of shale pore systems and further affecting the hydrocarbons production efficiency. In this work, two types of shales with different pyrite contents, namely, pyrite rich (PR, Niutitang Formation) and pyrite poor (PP, Xiamaling Formation), were emphasized to illustrate the effect of pyrite oxidation on pore structure after fracturing operation. Slickwater fracturing fluid was used to treat the shale samples for a period of 3 days, under the condition of 100 °C and 50 MPa. The field emission scanning electron microscopy (FE-SEM) and X-ray diffraction (XRD) were utilized to determine the surface morphology and mineral composition. The low-temperature N_2 adsorption was performed to quantify the pore structure. The

results showed that the pyrite oxidation induced the dissolution of both the pyrite and calcite and generated many dissolution pores for the pyrite-rich shale after slickwater treatment. The mineral dissolution led to an increase in the number of mesopores, enlarged the total specific surface area (TSSA) and total pore volume (TPV), and strengthened the pore-structure complexity. On the other hand, the pyrite-poor shale only experienced clay swelling after slickwater treatment. Its pore surface roughness and pore-structure complexity degraded with the loss of nanopores and the reductions in TSSA and TPV. The results of this study enhance the understanding of the impact of pyrite oxidation on the pore structure and provide new insight into the optimization of fracturing operation conditions based on shale's mineral composition characteristics.
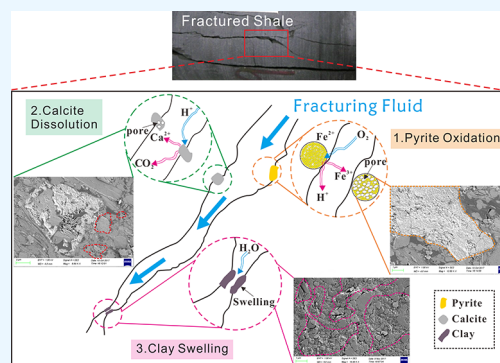
1. INTRODUCTION

As one of the unconventional natural gas resources, shale gas is altering the global energy consumption structure. In the past decades, shale gas exploration and development were mainly concentrated in the United States, China, Canada, and Argentina, with production levels in 2018 being 6.072×10^{11}, 1.09×10^{10}, 5.3×10^9, and 4.3×10^9 m^3, respectively.[1] The rapid increase in shale gas production around the world is attributed to the development of technologies in hydraulic fracturing and horizontal drilling. However, shale gas production decreases sharply after initial recovery from the hydraulically fractured wells.[2,3] One possible reason for the decrease in shale gas production is that the chemical reactions between minerals and fracturing fluid can alter the pore-structure characteristics of shale reservoirs.[4,5] Hydraulic fracturing introduces huge amounts of water-based fluid mixed with quartz sands and chemicals (7000−50 000 m^3 per well) to generate complex fracture networks and create fluid flow pathways.[6,7] After the fracturing operation is complete, only 20−40% of the injected fluid flows back and more than 60% remains in the subsurface.[8] The retained fracturing fluid can damage the pore throats and fractures of the shale formation.[9] Therefore, efforts to increase

shale gas production improve the importance of interactions between shale and injected fracturing fluid.

Shale as a kind of typical clay rock is primarily composed of clay minerals, brittle minerals (quartz, carbonates, feldspar, and chert), and easily oxidized components such as organic matter and pyrite.[10] Many researchers have revealed that the fracturing fluid chemically reacts with calcite, pyrite, and feldspar.[5,11−13] These chemical reactions can cause mineral dissolution and precipitation, alter rock properties, such as porosity and permeability, and further affect gas flow pathways within the shale matrix.[14] Thus, the relationship between geochemical shale-fracturing fluid interactions and the decline in shale gas production should be given more consideration. Herz-Thyhsen investigated the geochemical behavior of Al-bearing and Si-bearing minerals rock during simulated hydraulic fracturing
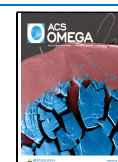
treatment and found that the calcite dissolution increased the porosity of calcareous mudstone by 37%.[2] Lu also presented that the calcite and dolomite dissolution created up to 28% surface porosity of shale after reacting with fracturing fluid.[12] Xiong reported that large euhedral barite (10−50 μm) precipitated on the shale fracture surface during the simulated injection period.[15]

As a common mineral in organic-rich shale, pyrite not only has an important effect on the shale gas enrichment[16] but also has the characteristics of easy oxidation under the oxygen environment.[17] It has been illustrated that pyrite has positive correlations with liquid hydrocarbon and total organic carbon (TOC), and it can promote the pyrolysis of organic matter and catalyze hydrocarbon generation.[18] Chen demonstrated that the pores within the pyrite framboids, which were as high as 5.66%, had a favorable contribution to the pore system of shale reservoir, and these pores could reserve free gas and promote gas enrichment.[19] In addition, the presence of pyrite in shale reservoirs can accelerate the oxidation of shale. A previous study indicated that most fracturing fluids contained dissolved oxygen (9 mg/L) and some oxidants, which were used as glue-breaking agents.[20] Although various oxygen scavengers and Fe-controlling agents are added to fracturing fluids to prevent the oxidative dissolution of pyrite, fracturing flow-back fluid normally contains large amounts of Fe in solution, indicating that these additives do not prevent pyrite oxidation effectively in reservoir conditions.[5] Xu observed that the dissolved oxygen in fracturing fluid can cause the pyrite oxidation and dissolution in shale through water imbibition experiments under oxic and degassed conditions.[21] The oxidation of pyrite has been considered one of the key factors that influence the shale pore structure.[5,11,22] Jew found that the Fe(II)-bearing phases could change to Fe(III)-bearing precipitates when the pH of fracturing fluid was above 3.25 in the carbonate-poor shale.[5] However, You reported that the oxidation of pyrite could produce dissolution pores and cracks, and the oxidation sensitivity was controlled by the pyrite content, dissolved oxygen content, and reservoir conditions.[23] Moreover, Li revealed that the pyrite oxidation zone was >0.5 cm into the shale matrix during hydraulic fracturing via synchrotron X-ray-based techniques, indicating that the pyrite oxidation occurred not only close to microfractures but also in a wider range of shale reservoir matrix.[24] Owing to the complex mineral composition in organic-rich shale, the mechanism of the pore structure change induced by pyrite oxidation is still not well-understood. Although most of the previous studies have demonstrated that the dissolution of pyrite has a significant effect on shale pore structure, little is known about the positive or negative effect of pyrite oxidation on pore-structure modification in shale reservoirs during hydraulic fracturing.

As a result, we performed laboratory experiments to confirm the positive or negative effect of pyrite oxidation on the pore-structure characteristics of shale during hydraulic fracturing. In this research, two shale samples with distinct pyrite content obtained from Niutitang Formation (pyrite rich) and the Xiamaling Formation (pyrite poor) were used for the fluid−shale interaction experiments. The surface morphology, mineral composition, and pore-structure characteristics of shale samples before and after fracturing fluid treatment were analyzed. The impact of pyrite oxidation on shale reservoir rocks was discussed, and the chemical influential mechanism of fluid−shale interaction on the shale pore structure was revealed. The results of this work will be helpful in optimizing hydraulic fracturing

operations for reservoirs with different mineralogical compositions and developing shale gas production.

2. MATERIAL AND METHODS

2.1. Shale Samples. Experimental shale samples used in this study were outcrops and obtained from Lower Cambrian Niutitang Formation (pyrite rich, labeled as PR) in the Youyang area of southeast Chongqing city and Mesoproterozoic Xiamaling Formation (pyrite poor, labeled as PP) in Chicheng area of northeast Hebei Province in China. These samples were selected due to their significant difference in pyrite content, and the basic information of the samples is shown in Table 1. Based

Table 1. Basic Information of Shale Samples Selected in This Study

| sample ID	TOC (wt %)	mineral composition (%)					
		quartz	pyrite	dolomite	calcite	feldspar	clay mineral
PR	8.4	65	8	1	1	11	14
PP	1.1	82					4	14

on the XRD results, the major minerals for PR shale are quartz (65%), clay mineral (14%), and pyrite (8%), while quarte (82%) and clay mineral (14%) are the dominant minerals for the PP shale. In addition to the different mineral compositions, the TOC content of the PR shale is 8.4 wt %, higher than that of 1.1 wt % for the PP shale.

Prior to the experiment, the outcrop block shale samples were cylindrically drilled to 25 mm in diameter and 50 mm in length. They were used for XRD and low-temperature nitrogen (N_2) adsorption tests before and after shale-fracturing fluid interaction. The thin slices of 2−3 cm^3 were prepared for FE-SEM measurement before and after the reaction. Considering that slickwater has been commonly used in shale gas production,[25] slickwater was also selected in this study. The physical property and chemical additives of the slickwater were reported in our previous study.[26]

2.2. Experiments and Methodology. To simulate the short-term influence of fracturing fluid on the pore structure of shale under the reservoir condition, the experiments were performed at reservoir temperature (100 °C) and pressure (50 MPa) for three days using a high-temperature and -pressure reaction device. The selection of temperature and pressure was ascribed to the burial depth of the PR and PP shale (2500−4000 m, the geothermal gradient is 20−25 °C/km) and the average pressure gradient of 0.015 MPa/m.[27−30]

The schematic diagram and main components of the simulation instrument have been described in detail in our previous study.[13] The experimental procedures were given as follows. The prepared shale samples were placed into the reactor. Then, fracturing fluid was injected and kept at the pressure of 50 MPa. The fluid/rock mass ratio was approximately 10:1. Finally, a heating system was performed. During the experiment, 10 mL of each solution was collected (24, 48, and 72 h), and the pH of the solution was monitored. After the reaction, the shale samples were cleaned using deionized water and heated to dry at 50 °C for 12 h in an oven to minimize the influence of free water and weakly bounded water in shale pores.[31] Then, they were collected for analyzing the mineralogy and pore-structure characteristics.

To better observe the mineral precipitation and dissolution at the water−rock interface, a Merlin Compact field emission
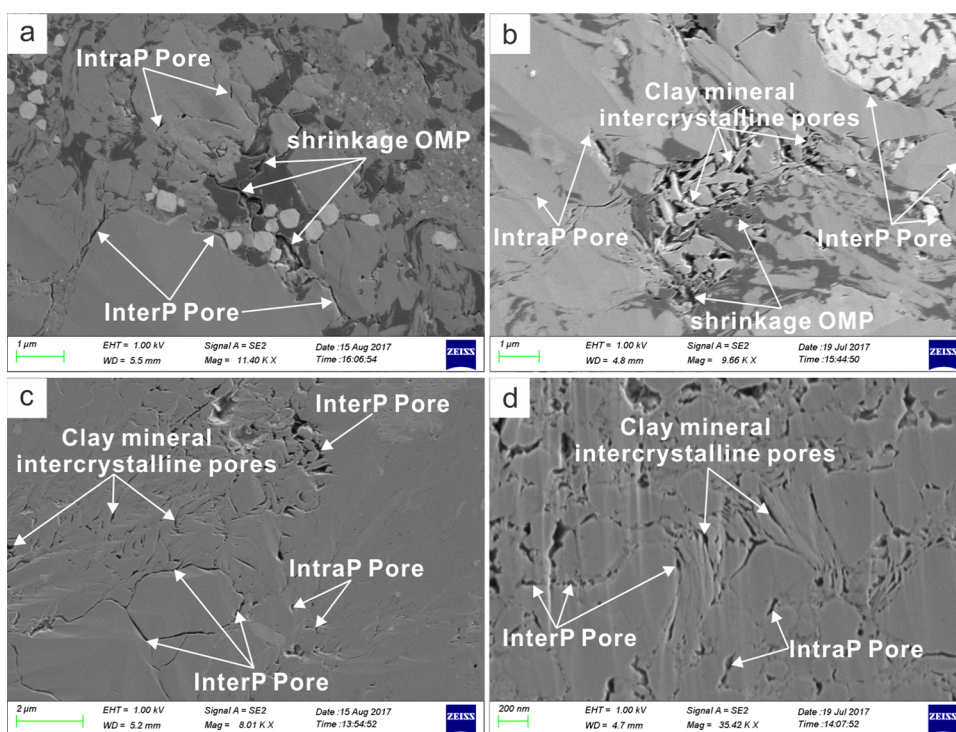
Figure 1. FE-SEM images of different pore types in the original PR (a, b) and PP (c, d) shale.
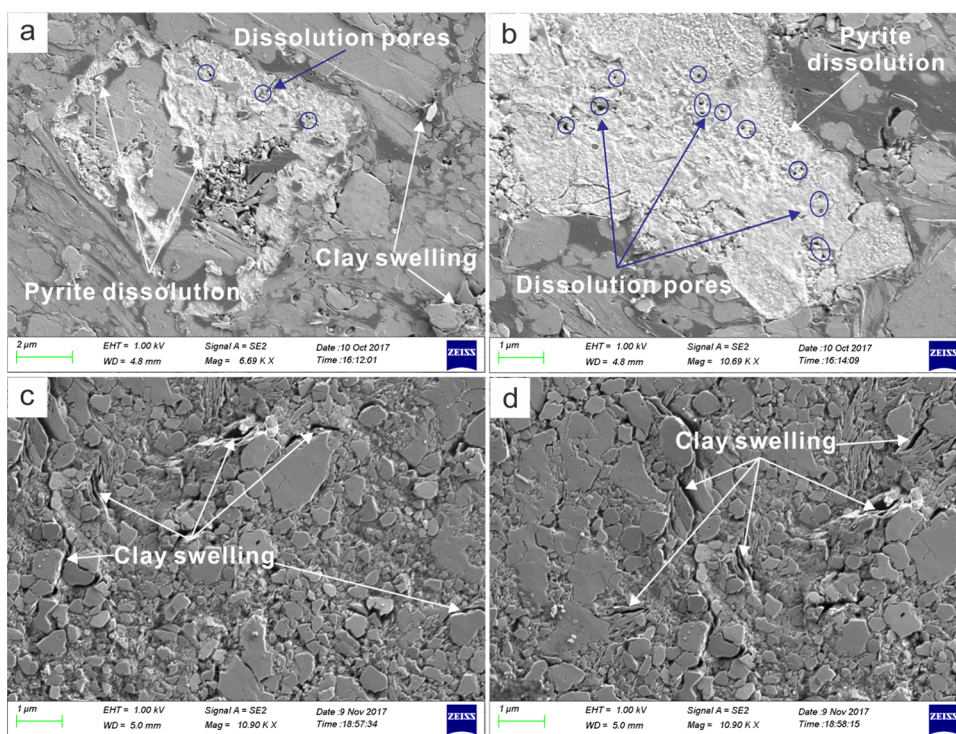
Figure 2. FE-SEM images of the fracturing fluid-reacted PR (a, b) and PP (c, d) shale.

scanning electron microscope (FE-SEM) with energy-dispersive spectroscopy (EDS) was applied to the image. Before the experiment, the thin slices of shale samples were ion milled to reduce the artifacts and roughness effect on the observation by an argon ion mill instrument (PECS II 685 C).

X-ray diffraction (XRD) analyses (Rigaku D/Max-III B X-ray diffractometer) were performed to measure the mineral composition of unreacted and reacted shale samples. The

cylindrical shale samples were crushed and passed through a 200 mesh sieve. The measurement was performed at 40 mA and 40 kV with Cu Kα radiation and scanned from 3 to 70° with a scanning rate of 2.0°/min.

To quantitatively analyze the pore evolution during hydraulic fracturing, a low-temperature N$_2$ adsorption test was implemented at the ASAP 2020 HD88 surface area analyzer. The unreacted and reacted shale samples were crushed to 40−60

Table 2. Mineralogical Compositions of the Unreacted and Reacted Shale Samples (%)

samples	state	quartz	pyrite	dolomite	calcite	feldspar	clay mineral
PR	unreacted	65	8	1	1	11	14
	reacted	66	6	1	0	11	16
PP	unreacted	82				4	14
	reacted	83				5	12

mesh, and the measurement process was identical to the study by Li which provided a detailed description.[32] The Brunauer−Emmett−Teller (BET) and Barrette−Joynere−Halenda (BJH) theories were used to calculate the specific surface area, pore volume, and pore size distribution.[33,34]

Based on the results of low-temperature N_2 adsorption, the fractal dimension (D) of the pore structure was calculated. The Frenkel−Halsey−Hill (FHH) model was used to calculate the value of D by applying eqs 1 and 2.[35,36]

$$\ln(V) = A \ln(\ln(P_0/P)) + C \qquad (1)$$

$$D = A + 3 \qquad (2)$$

where P_0 and P are the saturated vapor pressure and adsorption equilibrium pressure, respectively, MPa; V is the N_2 adsorption volume at P, cm³/g; A is the slope of the linear fitting curve; and C is the fitting constant. D, which ranges from 2 to 3, can be calculated based on eq 2.

3. RESULTS AND DISCUSSION

3.1. FE-SEM Imaging. Based on the FE-SEM, the variations in pore morphology and mineral composition on the shale surface were directly analyzed (Figures 1 and 2). The pore type in the original PR shale mainly consisted of interparticle (interP) pores developed among the edge of brittle mineral particles and intraparticle (intraP) pores within rigid particles (Figure 1a,b). In addition, the shrinkage organic matter pores (OMPs) (Figure 1a) and clay mineral intercrystalline pores (Figure 1b) were developed in the original PR shale. However, Figure 1c,d displays that the original PP shale contains many clay mineral intercrystalline pores and interP pores develop between clay and brittle mineral particles, as well as the intraP pores related to brittle mineral dissolution.

After the interaction experiments of slickwater fracturing fluid and shales, the changes in pore morphology and mineral composition on the shale surface are illustrated in Figure 2. Although the FE-SEM observation positions of the reacted shale are not the same as those of the unreacted shale, the qualitative analysis of the shale surface with similar morphology can still provide evidence of the changes on the surface of the matrix induced by water−rock interactions.[37] In the reacted PR shale, the original smooth surface of pyrite becomes rough, and pyrite shows obvious signs of erosion, which indicate that pyrite is dissolved and forms many dissolution pores within it. Meanwhile, clay swelling is also observed on its surface (Figure 2a,b). However, the original tight and flat shale surface of the PP shale matrix (Figure 1c,d) become expanded and looser after the slickwater treatment (Figure 2c,d), and the clay disintegration extends along the original clay mineral intercrystalline pores, which is closely related to the hydration expansion of the clay minerals.[38] The FE-SEM results indicate that the mineral composition has a significant effect on the pore structure of shale, and the reasons for the different variations of the two shale samples will be discussed later in this paper.

3.2. XRD Analysis. The changes in shale mineral composition before and after reaction with slickwater fracturing fluid are listed in Table 2. The analysis results suggested that the mineral compositions of the unreacted and reacted shale samples were different. In the PR shale, the contents of pyrite and calcite decreased by 25 and 100%, respectively (Table 2). Combined with the FE-SEM observation results of the PR shale, the content variations of pyrite and calcite indicated that the dissolution of these minerals might have occurred during the experiment. Moreover, the content of dolomite and feldspar in the PR shale did not change, and the slight increase in quartz and clay minerals might be attributed to partial mineral dissolution. However, the reacted PP shale showed similar mineral composition to the unreacted sample (Table 2). A previous study illustrated that the interaction between water-based fracturing fluid and shale could cause clay swelling,[39] which was in accordance with our results that the content of clay mineral decreased in the reacted PP shale. In addition, FE-SEM results of the reacted PP shale confirmed that the clay swelling occurred during the experiment.

Owing to the pH variation of the reaction fluid reflecting the degree of fluid−shale interaction, the pH of fracturing fluid discharged in different time periods (24, 48, and 72 h) was determined during the experiment (Figure 3). With the increase
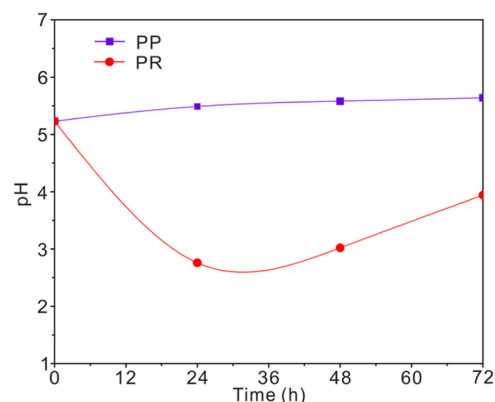
Figure 3. Variation of solutions pH during the reaction.

in reaction time, the pH of the aqueous solutions of the reacted PR and PP shale showed different trends. The pH for the PR shale remained acidic throughout the experiment, with a rapid decrease from 5.23 to 2.76 after 24 h and a gradual increase from 2.76 to 3.94 after 72 h. Nevertheless, the pH for the PP shale revealed a slight increase from pH 5.23 to 5.64 and provided an average value of 5.49 at the end of the experiment.

The results of pH and mineral composition changes in PR and PP shale suggested that different geochemical reactions occurred between shale and slickwater fracturing fluid. Previous studies confirmed that pyrite oxidation easily occurred in the environment of the atmosphere or water-containing oxygen.[22,40−42] The dissolved oxygen and the oxidative gel breakers in the fracturing fluid could have substantial effects on pyrite
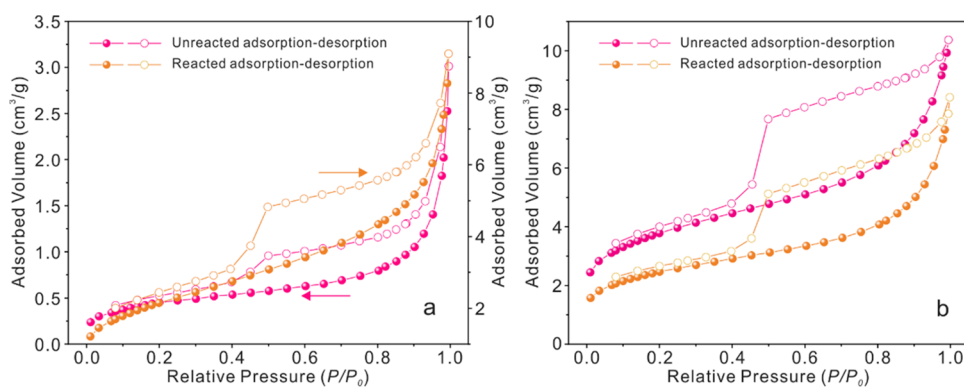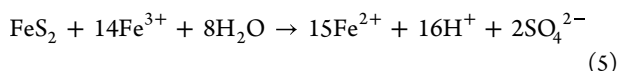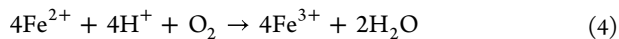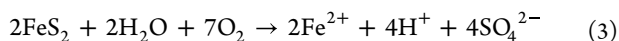
Figure 4. N_2 adsorption−desorption isotherms for the PR (a) and PP (b) shale sample.

Table 3. Pore-Structure Parameters of the Unreacted and Reacted Shale Samples[a]

samples	state	SSA (m²/g)				PV (cm³/g)				R_a (nm)
		micro-	meso-	macro-	TSSA	micro-	meso-	macro-	TPV	
PR	unreacted	0.378	1.061	0.050	1.489	0.00018	0.00254	0.00194	0.00466	12.521
	reacted	1.373	6.407	0.220	8.000	0.00062	0.00854	0.00507	0.01423	7.115
PP	unreacted	2.245	7.559	0.061	9.865	0.00105	0.01169	0.00200	0.01474	5.976
	reacted	1.438	4.990	0.164	6.592	0.00067	0.00768	0.00301	0.01136	6.893

[a]Note: micro-, meso-, and macro- represent micropores (<2 nm), mesopores (2−50 nm), and macropores (>50 nm), respectively. TSSA and TPV represent total SSA and total PV, respectively.

dissolution. The reactions of pyrite oxidation are represented as follows

$$2FeS_2 + 2H_2O + 7O_2 \rightarrow 2Fe^{2+} + 4H^+ + 4SO_4^{2-} \quad (3)$$

$$4Fe^{2+} + 4H^+ + O_2 \rightarrow 4Fe^{3+} + 2H_2O \quad (4)$$

$$FeS_2 + 14Fe^{3+} + 8H_2O \rightarrow 15Fe^{2+} + 16H^+ + 2SO_4^{2-} \quad (5)$$

Based on the results of FE-SEM, XRD, and solution pH, pyrite oxidation occurred in the PR shale during the experiment. The pyrite oxidation released H^+, which resulted in a sharp decrease in the solution pH after the reaction of slickwater and PR shale during the first 24 h, and a gradual increase in the pH toward the end indicated that pH buffering took place. The XRD results of PR shale showed that the calcite was not detected after the reaction, indicating that the acid produced by pyrite oxidation was gradually consumed by the dissolution of calcite. The geochemical reaction of PR shale may be shown as follows

$$4FeS_2 + 2H_2O + 15O_2 + 4CaCO_3$$
$$\rightarrow 4Fe^{3+} + 8SO_4^{2-} + 4Ca^{2+} + 4HCO_3^- \quad (6)$$
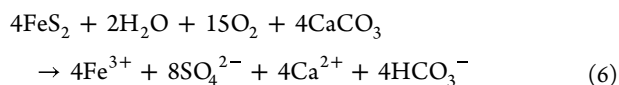
Owing to the main mineral of quartz and clay for the PP shale, the only geochemical reaction of the clay swelling occurred during the experiment.

3.3. Pore-Structure Analysis. *3.3.1. Characteristics of N_2 Adsorption−Desorption Isotherms.* Low-temperature N_2 adsorption−desorption isotherms of the unreacted and reacted PR and PP shale samples are shown in Figure 4. The hysteresis loops in N_2 isotherms were observed when the relative pressure (P/P_0) was higher than 0.45, reflecting that the capillary condensation occurred in the macropores (>50 nm) and mesopores (2−50 nm).[43] The hysteresis loops of untreated and reacted PR and PP shale were small, and the isotherms increased to infinity when $P/P_0 = 1$, which further reflected the existence of

macropores and mesopores in these shales.[44] Based on the IUPAC recommendation, the isotherm shapes and the hysteresis loops of the unreacted and reacted shale samples belonged to type IV and H2, respectively. The characteristics of N_2 adsorption−desorption isotherms indicated that the PR and PP shale possessed a continuous and open nanometer pore system, and pores in these shales were mainly slit pores and ink-bottle pores.[44,45]

As shown in Figure 4, some differences in the quantity of adsorbed N_2 at the highest pressure appeared for the PR and PP shale. The maximum amounts of adsorbed N_2 for the PR shale increased from 3.01 to 9.10 cm³/g after reaction with slickwater fracturing fluid (Figure 4a). However, a decrease in the maximum quantity of adsorbed N_2 from 10.37 to 7.85 cm³/g was observed for the PP shale (Figure 4b). The phenomenon illustrated that many nanopores were formed in the PR shale because the adsorption capacity of shale mainly depended on micropores (<2 nm) and mesopores (2−50 nm).[46] However, the nanopores were reduced in the PP shale after reaction with the slickwater fracturing fluid.

3.3.2. Changes in the Pore-Structure Parameters. The specific surface area (SSA), pore volume (PV), and average pore diameter (R_a) of unreacted and reacted shale samples were analyzed by the N_2 adsorption−desorption measurement, and the results are illustrated in Table 3. For the PR shale, the total SSA (TSSA) and total PV (TPV) increased greatly by 5.4 times and 3.1 times after reaction with fracturing fluid, respectively, but R_a decreased (Table 3). However, the TSSA, TPV, and R_a of sample PP showed completely opposite characteristics. The decreasing rates of TSSA and TPV were 33.2 and 22.9%, respectively, and the R_a increased from 5.976 to 6.893 nm. A previous study demonstrated that when the formation of new small pores was larger than the transformation degree of small pores to large pores, the R_a would show a decreasing trend.[31] To deeply explore the changed characteristics of micro-, meso-, and macropores before and after reaction with fracturing fluid, the
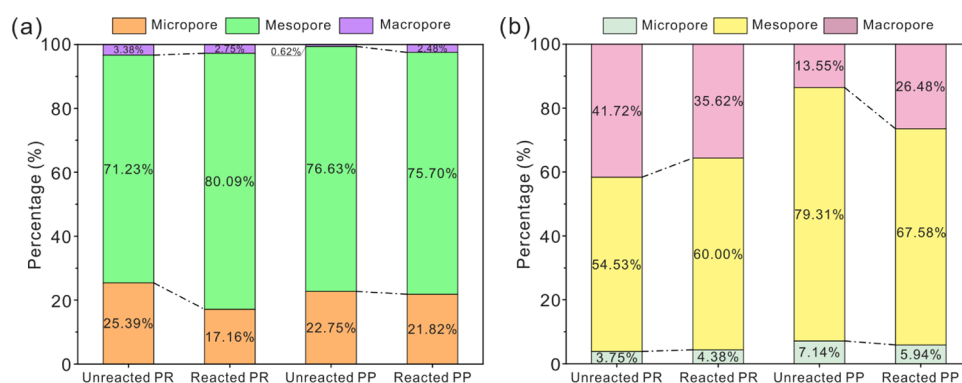
Figure 5. Percentages of micro-, meso-, macropores of SSA (a) and PV (b) before and after slickwater treatment.
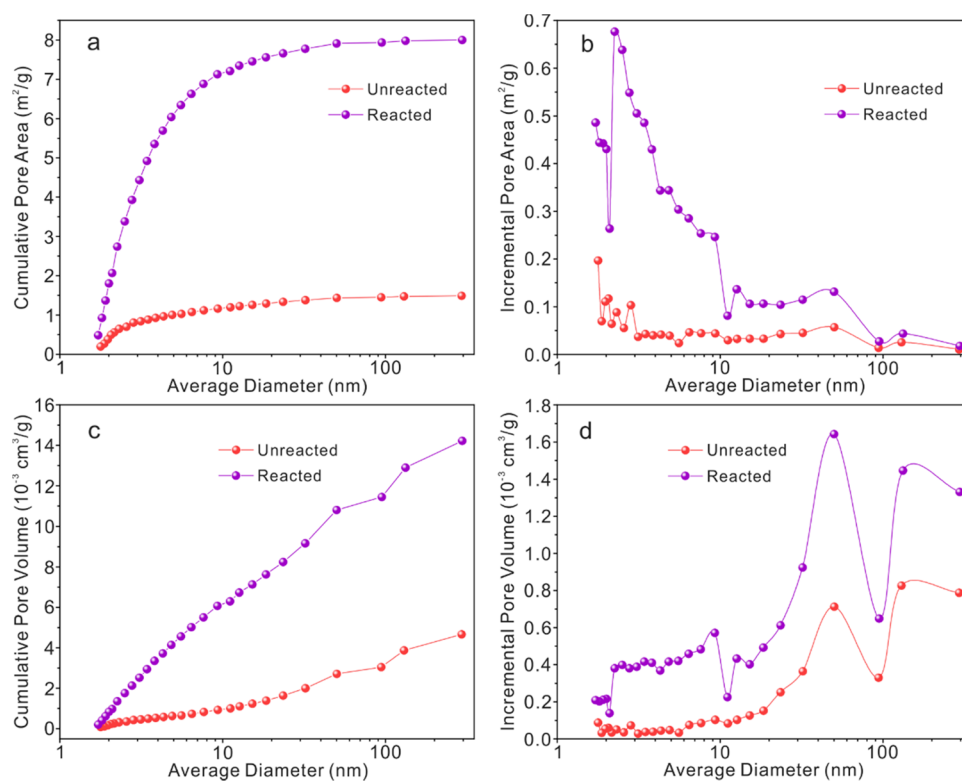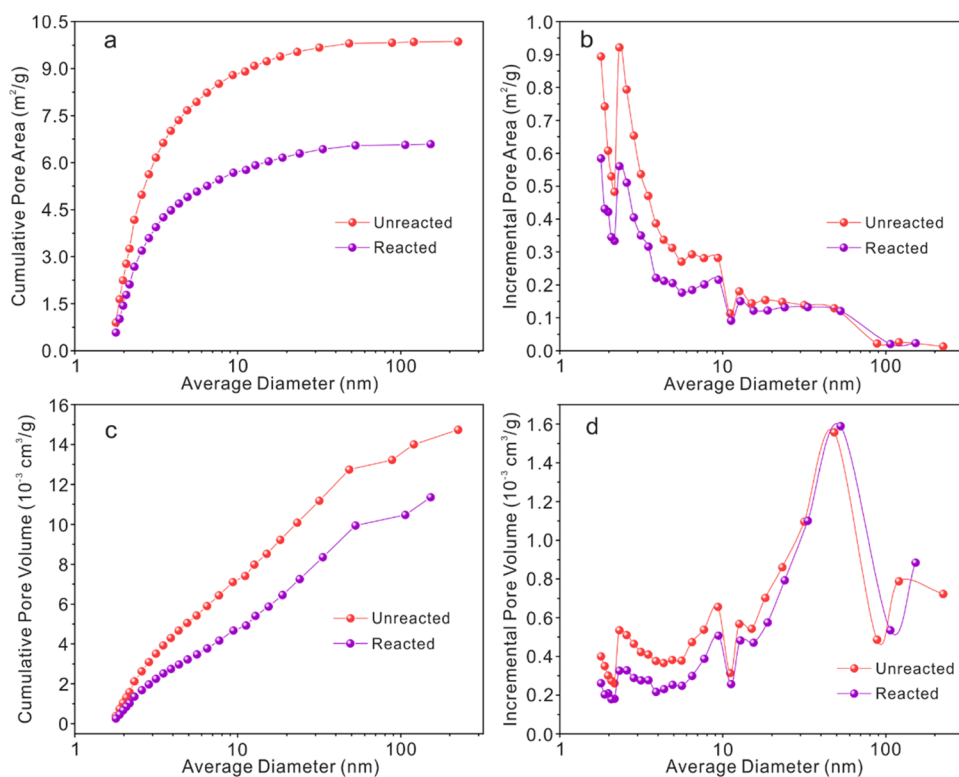

Figure 6. Pore area and volume distributions of the unreacted and reacted PR shale: (a) cumulative pore area; (b) pore area distribution corresponding to average pore diameter; (c) cumulative pore volume; and (d) pore volume distribution corresponding to average pore diameter.

percentage of each type of pore was calculated (Figure 5). The unreacted PR and PP shale mainly contained meso- and macropores, which provided more than 90% of the TPV. After slickwater treatment, the SSA and PV of the mesopores increased by 8.86 and 5.47% in PR shale, respectively. However, the SSA and PV of the mesopores decreased by 0.93 and 11.73% for the PP shale after reacting with fracturing fluid, respectively. These results illustrated that the variation in mesopores played a major role in the characteristics of pore structure change after slickwater treatment.

3.3.3. Evolution of Pore Area and Volume Distribution. To better reflect the distributions of SSA and PV for the PR and PP shale, their cumulative and incremental values were investigated. It could be seen that the cumulative pore area (Figure 6a) and pore volume (Figure 6c) gradually increased with the increase in the pore diameter of the PR shale. There was an obvious increase in cumulative pore area in the interval of 2−10 nm. Combined with the distribution characteristics of incremental pore area, it

was easy to find that the pore area of the reacted PR shale began to increase after 2 nm and had a peak at about 3 nm (Figure 6b). The results reflected that changed characteristics of pore area in the reacted PR shale were attributed to the increase in pores mainly occupied by mesopores with a diameter of 2−10 nm. Moreover, the pore volume of the PR shale experienced a significant increase after treatment with slickwater fracturing fluid (Figure 6c), which exhibited a trimodal feature at about 9.2, 50, and 132.9 nm (Figure 6d). These changes illustrated that the interactions between fracturing fluid and PR shale caused a more serious increase in pore volume especially the meso- and macropores, which was consistent with the analysis of pore-structure parameters. According to the previous research report, the pore area was mainly determined by small pores, while the pore volume was mainly by large pores;[31] thus, the pore area increased with the growing number of mesopores, and the pore volume increased with the growing number of meso- and macropores for the reacted PR shale.

Figure 7. Pore area and volume distributions of the unreacted and reacted PP shale: (a) cumulative pore area; (b) pore area distribution corresponding to average pore diameter; (c) cumulative pore volume; and (d) pore volume distribution corresponding to average pore diameter.

The pore area and volume distributions of the unreacted and reacted PP shale are displayed in Figure 7. After treatment with the slickwater fracturing fluid, the cumulative pore area (Figure 7a) and volume (Figure 7c) of the PP shale experienced a decrease. The incremental pore area of the reacted PP shale was significantly lower than that of unreacted in the range from 2 to 10 nm (Figure 7b). In addition, the variation in the incremental pore volume was concentrated in the pore interval below 10 nm (Figure 7d). These results indicated that the slickwater treatment mainly altered the mesopore structures of 2−10 nm, whereas it had little effect on the macropores of the PP shale.

3.4. Evolution of Pore Fractal Dimensions. According to eqs 1 and 2, the fractal parameters and fitting curves were obtained, as illustrated in Table 4 and Figure 8. Owing to the fact

Table 4. Fractal Dimensions of D_1 and D_2 of the Unreacted and Reacted Shale Samples

samples	state	P/P_0: 0−0.45		P/P_0: 0.45−1	
		D_1	R^2	D_2	R^2
PR	unreacted	2.507	0.962	2.664	0.997
	reacted	2.492	0.995	2.782	0.983
PP	unreacted	2.633	0.989	2.824	0.977
	reacted	2.620	0.988	2.785	0.982

that the gas adsorption mechanism at relative pressure below 0.45 was mainly monolayer or multilayer sorption, while at relative pressure above 0.45 was mainly capillary condensation.[47] Therefore, the D_1 and D_2 were calculated as the P/P_0 of 0−0.45 and 0.45−1 (Table 4). D_1 and D_2 showed a positive correlation with the pore surface roughness and pore structural complexity, respectively. The space structural irregularity and

heterogeneity of the pore surface and pore internal space could be quantitatively characterized.[48,49]

As shown in Table 4, the correlation coefficients (R^2) of all of the samples were large (>0.96), suggesting that the fractal dimensions of data fitting were reliable. Furthermore, the values of D_1 and D_2 ranged from 2 to 3, indicating that the pore structure of unreacted and reacted shale has good fractal properties. It can be seen that the D_1 of the PR and PP shale was slightly reduced after slickwater treatment, which reflected that the surface roughness of pores did not show any notable change. However, the D_2 variation of the PR and PP shale showed a different feature. For PR shale, the D_2 increased from 2.664 to 2.782, indicating that the slickwater treatment was able to enhance the pore structural complexity. For the PP shale, the D_2 decreased from 2.824 to 2.785, illustrating that the pore structure became more homogeneous after the reaction. Previous studies demonstrated that D_2 was positively related to the total specific surface and pore volume, while negatively related to average pore diameter.[31,50] As discussed above, the TSSA and TPV of the PR shale increased and R_a decreased after slickwater treatment, which was induced by the increase in mesopores. Thus, the growth in the number of mesopores in the PR shale led to an increase in the pore-structure complexity and a weakening in the pore connectivity. For the PP shale, the variations in D_1 and D_2 displayed good accordance with the pore-structure parameters, and the reduction of TSSA and TPV caused by clay swelling led to the decrease of pore surface roughness and pore-structure complexity.

3.5. Mechanism of Pore-Structure Change during Hydraulic Fracturing. According to the analysis results of the FE-SEM and XRD, the slickwater fracturing fluid can cause the oxidation of pyrite and the swelling of clay minerals. Therefore, the changes in pore structure were related to multiple
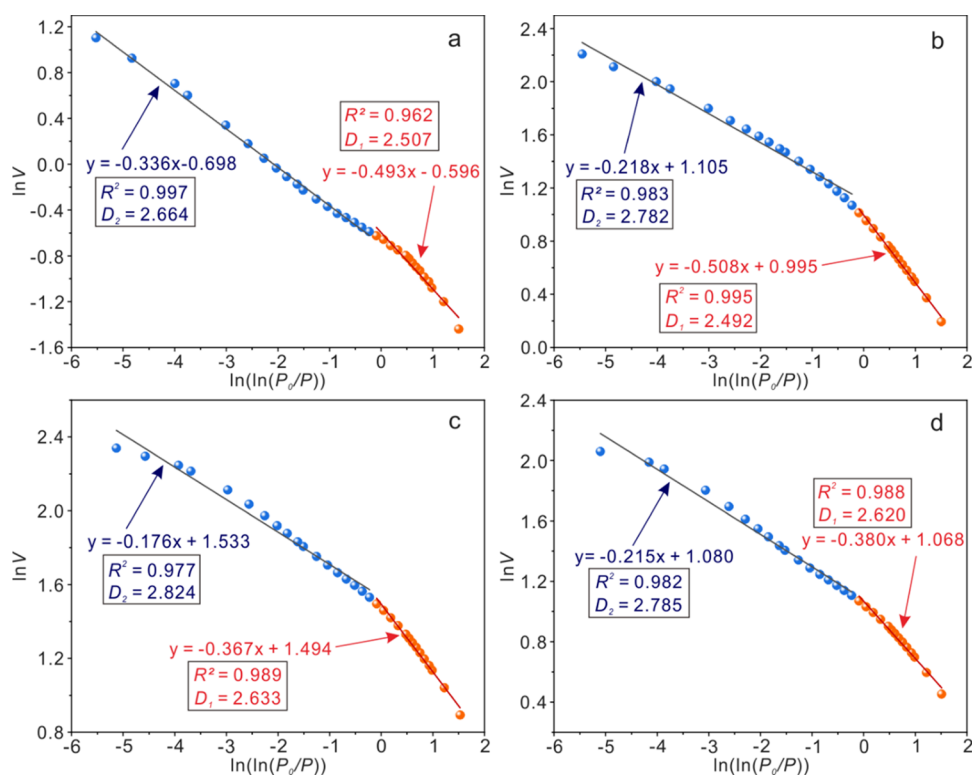
Figure 8. Fractal dimension features of PR (a: unreacted; b: reacted) and PP (c: unreacted; d: reacted) shale samples treated by slickwater fracturing fluid.
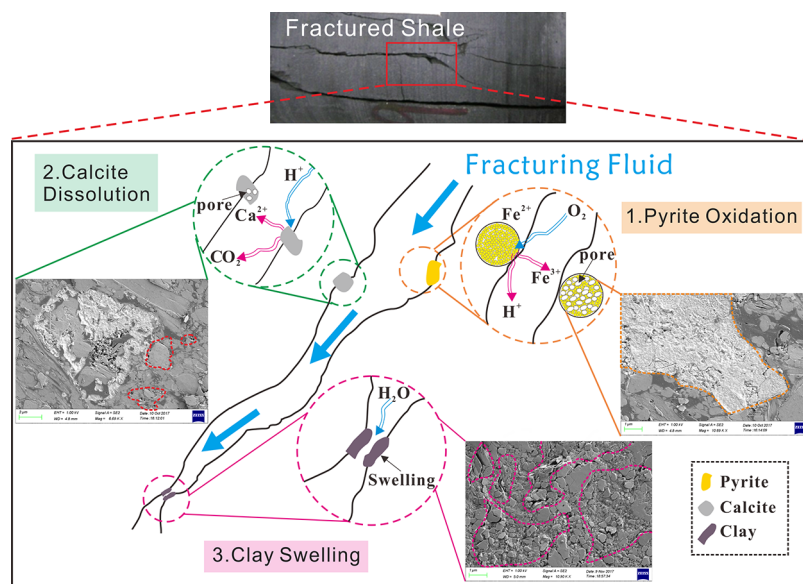
Figure 9. Schematic diagram of the reactions and results during hydraulic fracturing.

chemical reactions. A schematic diagram of the reactions and results during hydraulic fracturing is illustrated in Figure 9. Through comparison of the pyrite-rich and pyrite-poor shales, we found that the pyrite oxidation occurred, and then formed many dissolution pores and released H^+. The unstable minerals such as calcite in the shale could dissolve in the acidic solution, transforming micropores to meso- or macropores. Jew found that the release of Fe showed a steady increase in the carbonate-poor shale, while little to no Fe was detected in the carbonate-rich shale during 3 weeks of reaction,[5] which illustrated that the content of carbonates in shale had an obvious impact on pyrite oxidation. Due to the lower carbonate minerals of PR shale used in this study, pyrite dissolution occurred. Moreover, we found that the pyrite oxidation can cause an extensive increase in the mesopores in pyrite-rich shale, and the release of H^+ would also cause the dissolution of carbonate minerals, which thereby increased the TSSA and TPV and enhanced the pore-structure complexity. Therefore, it can be inferred that the pyrite oxidation during hydraulic fracturing can improve the number of mesopores in the shale gas reservoir, thereby having a favorable impact on gas production.

Meanwhile, the clay swelling could not be neglected during hydraulic fracturing. Previous studies illustrated that the illite/smectite, illite, and chlorite were the dominant clay minerals in the shale of Niutitang Formation and Xiamaling Formation.[29,51−53] The PR and PP shale containing clay minerals, which were dominated by swelling illite−smectite mixed-layer minerals, could easily lead to water-sensitive damage and hydration expansion after the fracturing operation.[38] The clay swelling could block the pore throats and reduce the connection between nanopores, which were identified by the results of the pore structure change of the PP shale. Therefore, pyrite oxidation and calcite dissolution caused by fracturing fluid treatment ultimately contributed to the increase in the number of nanopores especially the mesopores for PR shale, and the clay swelling led to the reduction in the number of nanopores for the PP shale.

4. CONCLUSIONS

In this study, by means of FE-SEM, XRD, and low-temperature N_2 adsorption, the mineral composition and nanopore structure characteristics evolution of two shales with different pyrite contents were examined before and after treatment of slickwater fracturing fluid. The major conclusions of this work are as follows:

(1) The FE-SEM and XRD results illustrated that the pyrite dissolved significantly in the PR shale after slickwater treatment, and the pyrite oxidation caused the pH of the solution to decrease, which further led to calcite dissolution. However, the main chemical reaction of the PP shale was clay swelling. The different reactions of shale minerals then caused a change in the pore structure.

(2) According to the low-temperature N_2 adsorption measurement, the TSSA and TPV significantly increased, while R_a decreased for the PR shale after the reaction. Nevertheless, the TSSA, TPV, and R_a of the PP shale showed completely different characteristics. The dissolution of pyrite and calcite resulted in an increase in the number of mesopores and the pore-structure complexity of the PR shale. The clay swelling reduced the pore volume and pore area of the PP shale and then led to the decrease in pore surface roughness and pore-structure complexity.

(3) Compared with the result of pore-structure characteristic of shale with different pyrite contents under fracturing operation, the mechanism of the pore structure change was revealed. The change in pore structure was related to the pyrite oxidation, calcite dissolution, and clay swelling. Moreover, this study documents sound evidence that pyrite oxidation has a favorable impact on the pore structure of shale during hydraulic fracturing.

■ AUTHOR INFORMATION

Corresponding Author

Yue Ni − *College of Resource and Environment, Shanxi Agricultural University, Jinzhong 030801, China*; Email: niyue2009@sina.cn

Authors

Zepeng Sun − *College of Resource and Environment, Shanxi Agricultural University, Jinzhong 030801, China*; ◉ orcid.org/0000-0002-0174-0487

Yuandong Wu − *Shenzhen Institute, Peking University, Shenzhen 518057, China*

Yong Lei − *College of Resource and Environment, Shanxi Agricultural University, Jinzhong 030801, China*

Complete contact information is available at: https://pubs.acs.org/10.1021/acsomega.2c02690

Notes

The authors declare no competing financial interest.

■ ACKNOWLEDGMENTS

■ REFERENCES

(1) Zou, C.; Yang, Z.; Sun, S.; Zhao, Q.; Bai, W.; Liu, H.; Pan, S.; Wu, S.; Yuan, Y. ″Exploring petroleum inside source kitchen″: Shale oil and gas in Sichuan Basin. *Sci. China: Earth Sci.* **2020**, *63*, 934−953.

(2) Herz-Thyhsen, R. J.; Kaszuba, J. P.; Dewey, J. C. Dissolution of minerals and precipitation of an aluminosilicate phase during experimentally simulated hydraulic fracturing of a mudstone and a tight sandstone in the Powder River Basin, WY. *Energy Fuels* **2019**, *33*, 3947−3956.

(3) Wachtmeister, H.; Lund, L.; Aleklett, K.; Hook, M. Production decline curves of tight oil wells in Eagle Ford Shale. *Nat. Resour. Res.* **2017**, *26*, 365−377.

(4) Herz-Thyhsen, R. J.; Kaszuba, J. P.; Dewey, J. C. Mineral dissolution and precipitation induced by hydraulic fracturing of a mudstone and a tight sandstone in the Powder River Basin, Wyoming, USA. *Appl. Geochem.* **2020**, *119*, No. 104636.

(5) Jew, A. D.; Dustin, M. K.; Harrison, A. L.; Joe-Wong, C. M.; Thomas, D. L.; Maher, K.; Brown, G. E., Jr; Bargar, J. R. Impact of organics and carbonates on the oxidation and precipitation of iron during hydraulic fracturing of shale. *Energy Fuels* **2017**, *31*, 3643−3658.

(6) Wang, F.; Chen, Q.; Lyu, X.; Zhang, S. Fracturing-fluid flowback simulation with consideration of proppant transport in hydraulically fractured shale wells. *ACS Omega* **2020**, *5*, 9491−9502.

(7) Vengosh, A.; Jackson, R. B.; Warner, N.; Darrah, T. H.; Kondash, A. A critical review of the risks to water resources from unconventional shale gas development and hydraulic fracturing in the United States. *Environ. Sci. Technol.* **2014**, *48*, 8334−8348.

(8) Hu, Y.; Zhao, C.; Zhao, J.; Wang, Q.; Zhao, J.; Gao, D.; Fu, C. Mechanisms of fracturing fluid spontaneous imbibition behavior in shale reservoir: A review. *J. Nat. Gas Sci. Eng.* **2020**, *82*, No. 103498.

(9) Khan, H. J.; Spielman-Sun, E.; Jew, A. D.; Bargar, J.; Kovscek, A.; Druhan, J. L. A Critical review of the physicochemical impacts of water chemistry on shale in hydraulic fracturing systems. *Environ. Sci. Technol.* **2021**, *55*, 1377−1394.

(10) You, L.; Cheng, Q.; Kang, Y.; Chen, Q.; Dou, L.; Zhou, Y. Imbibition of oxidative fluid into organic-rich shale: Implication for oxidizing stimulation. *Energy Fuels* **2018**, *32*, 10457−10468.

(11) Harrison, A. L.; Jew, A. D.; Dustin, M. K.; Thomas, D. L.; Joe-Wong, C. M.; Bargar, J. R.; Johnson, N.; Brown, G. E.; Maher, K.

Element release and reaction-induced porosity alteration during shale-hydraulic fracturing fluid interactions. *Appl. Geochem.* **2017**, *82*, 47−62.

(12) Lu, J.; Mickler, P. J.; Jean-Philippe, N.; Wanjoo, C.; Esch, W. L.; Roxana, D. Geochemical interactions of shale and brine in autoclave experiments-Understanding mineral reactions during hydraulic fracturing of Marcellus and Eagle Ford Shales. *AAPG Bull.* **2017**, *101*, 1567−1597.

(13) Sun, Z.; Zhang, H.; Wei, Z.; Wang, Y.; Wu, B.; Zhuo, S.; Zhao, Z.; Li, J.; Hao, L.; Yang, H. Effects of slick water fracturing fluid on pore structure and adsorption characteristics of shale reservoir rocks. *J. Nat. Gas Sci. Eng.* **2018**, *51*, 27−36.

(14) Li, Q.; Jew, A. D.; Brown, G. E.; Bargar, J. R.; Maher, K. Reactive transport modeling of shale-fluid interactions after imbibition of fracturing fluids. *Energy Fuels* **2020**, *34*, 5511−5523.

(15) Xiong, W.; Gill, M.; Moore, J.; Crandall, D.; Hakala, J. A.; Lopano, C. Influence of reactive flow conditions on barite scaling in Marcellus Shale during stimulation and shut-in periods of hydraulic fracturing. *Energy Fuels* **2020**, *34*, 13625−13635.

(16) Chen, X.; Chen, L.; Tan, X.; Jiang, S.; Wang, C. Impact of pyrite on shale gas enrichment-a case study of the Lower Silurian Longmaxi Formation in southeast Sichuan Basin. *Fornt. Earth Sci.* **2021**, *15*, 332−342.

(17) Elie, M.; Faure, P.; Michels, R.; Landais, P.; Griffault, L. Natural and laboratory oxidation of low-organic-carbon-content sediments: Comparison of chemical changes in hydrocarbons. *Energy Fuels* **2000**, *14*, 854−861.

(18) Cao, T. T.; Deng, M.; Song, Z. G.; Liu, G. X.; Huang, Y. R.; Hursthouse, A. S. Study on the effect of pyrite on the accumulation of shale oil and gas. *Nat. Gas Geosci.* **2018**, *29*, 404−414.

(19) Chen, X.; Chen, L.; Tan, X.; Wang, C.; Ji, Y.; Xiong, M.; Wang, G. Pore characterization of pyrite in the Longmaxi Formation shale in the Upper Yangtze Area of China. *Front. Earth Sci.* **2022**, *10*, No. 848247.

(20) Yuan, B.; Wood, D. A. A comprehensive review of formation damage during enhanced oil recovery. *J. Pet. Sci. Eng.* **2018**, *167*, 287−299.

(21) Xu, M.; Binazadeh, M.; Zolfaghari, A.; Dehghanpour, H. Effects of dissolved oxygen on water imbibition in gas shales. *Energy Fuels* **2018**, *32*, 4695−4704.

(22) Vandeginste, V.; Siska, A.; Belshaw, G.; Kilpatrick, A. Effect of salinity on the kinetics of pyrite dissolution in oxygenated fluids at 60 °C and implications for hydraulic fracturing. *J. Nat. Gas Sci. Eng.* **2021**, *86*, No. 103722.

(23) You, L.; Zhou, Y.; Kang, Y.; Cheng, Q.; Zhang, N. Experimental evaluation of oxidation sensitivity in organic-rich shale reservoir. *J. Pet. Sci. Eng.* **2020**, *192*, No. 107230.

(24) Li, Q.; Jew, A. D.; Kohli, A.; Maher, K.; Brown, G. E.; Bargar, J. R. Thicknesses of chemically altered zones in shale matrices resulting from interactions with hydraulic fracturing fluid. *Energy Fuels* **2019**, *33*, 6878−6889.

(25) Sahai, R.; Moghanloo, R. G. Proppant transport in complex fracture networks-A review. *J. Pet. Sci. Eng.* **2019**, *182*, No. 106199.

(26) Sun, Z.; Wang, Y.; Wei, Z.; Ni, Y.; Wu, B.; Li, J.; Fan, W.; Wang, G.; Li, Y. Pore structure alteration characteristics of different mineralogical composition shale during shale-fracturing fluid physical-chemical interactions. *Geofluids* **2019**, *2019*, 1−13.

(27) Wang, P.; Yao, S.; Jin, C.; Li, X.; Zhang, K.; Liu, G.; Zang, X.; Liu, S.; Jiang, Z. Key reservoir parameter for effective exploration and development of high-over matured marine shales: A case study from the cambrian Niutitang formation and the silurian Longmaxi formation, south China. *Mar. Pet. Geol.* **2020**, *121*, No. 104619.

(28) Li, X.; Chen, S.; Wang, X.; Zhu, Y.; Chang, M.; Uwamahoro, C. Pore structure heterogeneity of the Xiamaling Formation shale gas reservoir in the Yanshan area of China: evaluation of geological controlling factors. *Acta Geol. Sin. (Engl. Ed.)* **2019**, *93*, 588−603.

(29) Xu, L.; Yang, K.; Wei, H.; Liu, L.; Jiang, Z.; Li, X.; Chen, L.; Xu, T.; Wang, X. Pore evolution model and diagenetic evolution sequence of the Mesoproterozoic Xiamaling shale in Zhangjiakou, Hebei. *J. Pet. Sci. Eng.* **2021**, *207*, No. 109115.

(30) Yin, H.; Zhou, J.; Jiang, Y.; Xian, X.; Liu, Q. Physical and structural changes in shale associated with supercritical CO$_2$ exposure. *Fuel* **2016**, *184*, 289−303.

(31) Lu, Y.; Liu, J.; Tang, J.; Ao, X.; Li, H.; Zhou, J.; Sun, X. Pore changes of slickwater-containing shale under supercritical CO$_2$ treatment. *Fuel* **2022**, *312*, No. 122775.

(32) Li, J.; Zhou, S. X.; Li, Y. J.; Ma, Y.; Yang, Y. A.; Li, C. Effect of organic matter on pore structure of mature lacustrine organic-rich shale: A case study of the Triassic Yanchang shale, Ordos Basin, China. *Fuel* **2016**, *185*, 421−431.

(33) Barrett, E. P.; Joyner, L. G.; Halenda, P. P. The determination of pore volume and area distributions in porous substances. 1. computations from nitrogen isotherms. *J. Am. Chem. Soc.* **1951**, *73*, 373−380.

(34) Brunauer, S.; Emmett, P. H.; Teller, E. Adsorption of gases in multimolecular layers. *J. Am. Chem. Soc.* **1938**, *60*, 309−319.

(35) Pfeifer, P.; Avnir, D. Chemistry in noninteger dimensions between two and three. 1. fractal theory of heterogeneous surfaces. *J. Chem. Phys.* **1983**, *79*, 3558−3565.

(36) Sakhaee-Pour, A.; Li, W. Fractal dimensions of shale. *J. Nat. Gas Sci. Eng.* **2016**, *30*, 578−582.

(37) Zeng, L.; Akhondzadeh, H.; Iqbal, M. A.; Keshavarz, A.; Rezaee, R.; Xie, Q. Effect of fluid-shale interactions on shales micromechanics: Nanoindentation experiments and interpretation from geochemical perspective. *J. Nat. Gas Sci. Eng.* **2022**, *101*, No. 104545.

(38) Wang, B.; Liu, B.; Yang, J.; Bai, L.; Li, S. Compatibility characteristics of fracturing fluid and shale oil reservoir: A case study of the first member of Qingshankou Formation, Northern Songliao Basin, Northeast China. *J. Pet. Sci. Eng.* **2022**, *211*, No. 110161.

(39) Zhou, Z.; Abass, H.; Li, X. P.; Teklu, T. Experimental investigation of the effect of imbition on shale permeability during hydraulic fracturing. *J. Nat. Gas Sci. Eng.* **2016**, *29*, 413−430.

(40) Kameia, G.; Ohmotob, H. The kinetics of reactions between pyrite and O$_2$-bearing water revealed from in situ monitoring of DO, Eh and pH in a closed system. *Geochim. Cosmochim. Acta* **2000**, *64*, 2585−2601.

(41) Moses, C. O.; Herman, J. S. Pyrite oxidation at circumneutral pH. *Geochim. Cosmochim. Acta* **1991**, *55*, 471−482.

(42) Williamson, M. A.; Rimstidt, J. D. The kinetics and electrochemical rate-determining step of aqueous pyrite oxidation. *Geochim. Cosmochim. Acta* **1994**, *58*, 5443−5454.

(43) Chen, X.; Qu, X.; Xu, S.; Wang, W.; Li, S.; He, H.; Liu, Y. Dissolution pores in shale and their influence on reservoir quality in Damintun Depression, Bohai Bay Basin, East China: Insights from SEM images, N$_2$ adsorption and fluid-rock interaction experiments. *Mar. Pet. Geol.* **2020**, *117*, No. 104394.

(44) Bai, L.-H.; Liu, B.; Du, Y.-J.; Wang, B.-Y.; Tian, S. S.; Wang, L.; Xue, Z. Distribution characteristics and oil mobility thresholds in lacustrine shale reservoir: Insights from N$_2$ adsorption experiments on samples prior to and following hydrocarbon extraction. *Pet. Sci.* **2022**, *19*, 486−497.

(45) Sing, K. S.; Everett, D. H.; Haul, R. A.; Moscou, L.; Pierotti, R. A.; Rouquerol, J. J.; Siemieniewska, T. Reporting physisorption data for gas solid systems with special reference to the determination of surface-area and porosity (recommendations 1984). *Pure Appl. Chem.* **1985**, *57*, 603−619.

(46) Wang, Y.; Liu, L. F.; Hu, Q.; Hao, L.; Wang, X.; Sheng, Y. Nanoscale pore network evolution of Xiamaling marine shale during organic matter maturation by hydrous pyrolysis. *Energy Fuels* **2020**, *34*, 1548−1563.

(47) Xue, S.; Huang, Q.; Wang, G.; Bing, W.; Li, J. Experimental study of the influence of water-based fracturing fluids on the pore structure of coal. *J. Nat. Gas Sci. Eng.* **2021**, *88*, No. 103863.

(48) Liu, X.; Xiong, J.; Liang, L. Investigation of pore structure and fractal characteristics of organic-rich Yanchang formation shale in central China by nitrogen adsorption/desorption analysis. *J. Nat. Gas Sci. Eng.* **2015**, *22*, 62−72.

(49) Wood, D. A. Estimating organic-rich shale fractal dimensions from gas adsorption isotherms: combining different methods leads to more reliable values and insight. *Nat. Resour. Res.* **2021**, *30*, 3551−3574.

(50) Liang, L.; Xiong, J.; Liu, X. An investigation of the fractal characteristics of the Upper Ordovician Wufeng Formation shale using nitrogen adsorption analysis. *J. Nat. Gas Sci. Eng.* **2015**, *27*, 402−409.

(51) Cao, X.; Yu, B.; Li, X.; Sun, M.; Zhang, L. Reservoir characteristics and well-logging evaluation of the Lower Cambrian shales in southeast Chongqing, China. *Pet. Res.* **2016**, *1*, 178−190.

(52) Wang, B.; Zhang, Q.; Wang, G.; Liu, M. Analysis on the difference of material composition and reservoir space of Mesoproterozoic dark marine shale in the Yanshan area. *Energy Explor. Exploit.* **2019**, *37*, 332−354.

(53) Xi, Z.; Tang, S.; Zhang, S.; Lash, G. G.; Ye, Y. Controls of marine shale gas accumulation in the eastern periphery of the Sichuan Basin, South China. *Int. J. Coal Geol.* **2022**, *251*, No. 103939.